Excitons bound to isoelectronic Te traps in ZnSe quantum wells: A theoretical study

G.T. Einevoll
Institutt for Fysikk, Norges Tekniske Høgskole, Universitetet i Trondheim, N-7034 Trondheim, Norway

D.S. Citrin and Yia-Chung Chang
Department of Physics and Materials Research Laboratory, University of Illinois at Urbana-Champaign, 1110 West Green Street, Urbana, Illinois 61801

(Received 12 February 1991)

A theoretical study is made of excitons and holes bound to a single tellurium (Te) impurity in bulk ZnSe and centered in ZnSe-$Zn_{1-x}Mn_xSe$ strained quantum wells. We use an effective-bond-orbital model for the holes in order to account for the complicated valence-band structure, and the spherical effective-mass approximation to describe the electron. The mutual Coulomb interaction is included, and solutions for the two-body system are obtained using the variational method in an iterative scheme. The strong lattice-relaxation effects present in the binding of the hole to the Te impurity are absorbed in the value for the localized hole-attractive potential at the site of the impurity. This value is determined by fitting the experimental value for the binding energy of the bound exciton. The oscillator strengths, the extension of the bound-exciton wave functions, and the energies of bound holes are then predicted. We observe a discrepancy between the fitted value for the localized impurity potential for the bulk case and the quantum-well case. An experiment to test our explanation for the discrepancy is proposed.

I. INTRODUCTION

An isoelectronic impurity is an impurity which has the same valence-electron structure, but different core-electron structure, from the atom it substitutes. Trapping of excitons by isoelectronic impurities is a phenomenon which often must be taken into account when explaining optical spectra from semiconductor samples. One of the most studied cases is gallium phosphide doped with nitrogen (GaP:N). The N impurity is attractive for electrons, and the binding of the exciton is commonly visualized as follows:[1] An electron is trapped in the short-range isoelectronic potential of the impurity, and a hole is bound in the Coulomb field resulting from the electron. This description suggests that an exciton cannot be bound by the impurity unless the electron itself is bound. The situation turns out to be more complicated however (see Ref. 2 and references therein). While for GaP:N the bound exciton has a binding energy of 28 meV, which is considerably larger than the free-exciton binding energy of 20 meV, a detailed theoretical study found the electron to be barely bound with a binding energy of less than 1 meV.[1] This suggests that systems may occur which display bound excitons even if the electron does not bind by itself.

Another system which has attracted considerable interest is tellurium-doped zinc selenide (ZnSe:Te) where Te acts as an isoelectronic impurity attractive for holes.[3–8] Depending on the Te concentration this system exhibits different trapping mechanisms. For large impurity concentrations no distinct gap between localized and delocalized excitons is observed, and the localized exciton states seem to be best described in terms of binding to a random potential due to large-scale compositional fluctuations.[3] For small Te concentrations photoluminescence spectra reveal isolated peaks which are best understood in terms of localization of excitons at small clusters of Te atoms.[3–5,7] In a recent experimental study Lee *et al.*[7] performed photoluminescence measurements on single crystal $ZnTe_xSe_{1-x}$ with $x \simeq 0.01$, for a set of different temperatures. Two broad peaks, red-shifted by more than 100 meV compared to the free-exciton peak, dominated the spectra. The peaks were explained as resulting from recombination of excitons bound to single and neighboring pairs of Te atoms, respectively. Later, Fu *et al.*[8] extended the study to ZnSe-$Zn_{1-x}Mn_xSe$ strained quantum wells with Te impurities in the middle and, in addition to confirming previous findings in Ref. 7, demonstrated that the hole wave function is strongly localized around the Te sites. The peak assigned to excitons bound to single Te atoms was also observed in earlier photoluminescence studies by Naumov *et al.*[3] and Reznitsky *et al.*[4] The interpretations of the peaks differ, however. Citing cathodoluminescence work by Akimova *et al.*,[5] Reznitsky *et al.* assigned the same peak to recombination of excitons bound to a cluster of three Te atoms. Furthermore, a small spectral feature at the high-energy side was assigned to excitons bound to pairs of Te atoms. A generally accepted understanding of the physical situation thus seems lacking.

The qualitative picture that has emerged for bound excitons in ZnSe:Te is a hole strongly bound to a short-range isoelectronic potential with an electron bound in a larger orbit in the Coulomb field from the hole. The exci-

ton trapping involves electron-phonon interactions which induce a locally distorted lattice around the Te impurity.

A determination of the shape and strength of the short-range isoelectronic potential from microscopic considerations is very difficult and has prohibited accurate first-principle calculations of the exciton binding energy. The most elaborate calculations on isoelectronic traps so far were performed on GaP:N. Masselink and Chang[1] calculated the exciton binding energy of this system taking into account the band structures for both electron and hole and their mutual Coulomb interaction. The short-range potential was fitted to give the experimentally observed exciton binding energy, and the electron binding energy could thus be predicted. The method was later extended to include bound-exciton molecules.[2]

In this paper we present results of a theoretical study of excitons and holes bound to a single Te impurity in bulk ZnSe and a single Te impurity centered in a ZnSe-$Zn_{0.79}Mn_{0.21}Se$ strained quantum well. We use the effective-bond-orbital model[9] (EBOM) for the holes in order to account properly for the complicated valence-band structure. The electron is described by the spherical effective-mass approximation. The mutual Coulomb interaction is included, and solutions for the two-body system are obtained using the variational method in an iterative scheme. The strong lattice-relaxation effects are absorbed into the value for the localized potential at the site of the isoelectronic impurity. This value is determined by fitting the experimental value for the binding energy of the bound exciton. Other quantities, such as the binding energy for a bound hole, the oscillator strength, and the extension of the bound-exciton wave function, are then predicted.

In Sec. II we describe our method. In Secs. III and IV we present results for bound excitons and holes trapped by Te impurities in bulk ZnSe and ZnSe-$Zn_{1-x}Mn_xSe$ quantum wells, respectively, and compare with available experimental data. Discussion and some concluding remarks are given in Sec. V.

II. THEORY

In the present work we calculate properties of bound excitons in bulk and in quantum wells. Since bulk can be regarded as a special case of a quantum well, it suffices to consider excitons and holes bound to a Te impurity centered in a quantum well. The model Hamiltonian we use for an exciton bound to an isoelectronic impurity in a quantum well is

$$H = H_h(\nabla_h, \mathbf{r}_h) + V(\mathbf{r}_h) + H_e(\nabla_e, \mathbf{r}_e) + v(|\mathbf{r}_h - \mathbf{r}_e|), \quad (1)$$

where H_h (H_e) is the Hamiltonian for a hole (electron) seeing the quantum-well potential only, and $V(\mathbf{r}_h)$ is a short-range attractive potential for the hole due to the Te impurity at the center of the well. The analogous repulsive potential for the electron is ignored in the present calculations.[10] The last term in Eq. (1), $v(|\mathbf{r}_h - \mathbf{r}_e|)$, accounts for the attractive Coulomb interaction between electron and hole.

The bound-exciton energy E is found by minimizing

$$< \Psi(\mathbf{r}_e, \mathbf{r}_h)|H|\Psi(\mathbf{r}_e, \mathbf{r}_h) >= E < \Psi(\mathbf{r}_e, \mathbf{r}_h)|\Psi(\mathbf{r}_e, \mathbf{r}_h) > \quad (2)$$

using a self-consistent Hartree scheme ignoring the electron-hole exchange interaction.[11] The two-particle wave function is assumed separable, i.e., $\Psi(\mathbf{r}_e, \mathbf{r}_h) = \psi_e(\mathbf{r}_e)\psi_h(\mathbf{r}_h)$. This approximation is best for situations where the hole is strongly localized at the impurity. For GaP:N the error introduced by assuming separability was estimated[2] for a simpler model by comparing results using a separable wave function with results using a more complicated (nonseparable) trial wave function which exhibits the correct limiting form for very shallow impurity potentials (free-exciton wave function). For situations where an isolated electron is bound by the isoelectronic N trap, the error introduced was found to be less than 6%.

With a separable wave function (2) simplifies to

$$\frac{< \psi_h|H_h + V|\psi_h >}{< \psi_h|\psi_h >} + \frac{< \psi_e|H_e|\psi_e >}{< \psi_e|\psi_e >} + \frac{< \psi_h\psi_e|v|\psi_e\psi_h >}{< \psi_h|\psi_h >< \psi_e|\psi_e >} = E . \quad (3)$$

The bound-exciton energy is found iteratively by consecutively minimizing, by solving secular equations for appropriate sets of basis functions,

$$\frac{< \psi_h^n|H_h + V + V_{\text{eff}}^e|\psi_h^n >}{< \psi_h^n|\psi_h^n >} = E_h , \quad (4)$$

where

$$V_{\text{eff}}^e = V_{\text{eff}}^e(\mathbf{r}_h) \equiv \frac{< \psi_e^{n-1}|v|\psi_e^{n-1} >}{< \psi_e^{n-1}|\psi_e^{n-1} >} , \quad (5)$$

with $|\psi_e^{n-1}>$ fixed, and

$$\frac{< \psi_e^n|H_e + V_{\text{eff}}^h|\psi_e^n >}{< \psi_e^n|\psi_e^n >} = E_e , \quad (6)$$

where

$$V_{\text{eff}}^h = V_{\text{eff}}^h(\mathbf{r}_e) \equiv \frac{< \psi_h^n|v|\psi_h^n >}{< \psi_h^n|\psi_h^n >} , \quad (7)$$

with $|\psi_h^n>$ fixed until the values for E_h and E_e have converged. Here $|\psi_e^n>$ ($|\psi_h^n>$) is the electron (hole) wave function after the nth iteration, and V_{eff}^e (V_{eff}^h) is the so-called Hartree potential felt by the hole (electron) due to the electron (hole) charge density. After convergence the exciton binding energy is given by

$$E = E_h + E_e - \frac{< \psi_e\psi_h|v|\psi_h\psi_e >}{< \psi_h|\psi_h >< \psi_e|\psi_e >} . \quad (8)$$

The binding energy for the hole alone is found by solving Eq. (4) without the term due to the electron-hole interaction.

The rest of the theory section is organized in four subsections. In II A the evaluation of the matrix elements

involving $H_h + V$ in Eq. (4), which corresponds to solving the pure hole problem, is described. The formalism involved in describing the electron is outlined in II B while the incorporation of the electron-hole interaction is given in II C. The separate pieces from Secs. II A–II C are joined together in II D to give a procedure for calculating exciton binding energies. Our study also includes calculations of oscillator strengths and average hole and electron distances from the impurity, and a brief description of how to extract these quantities is also included in II D.

A. Holes

We first discuss how a hole interacting with a single isoelectronic impurity centered in a quantum well is described within the EBOM formalism. The EBOM has previously been used to calculate binding energies of acceptors centered in quantum wells,[12] and this treatment is readily extended to the present application. In the presentation below we will briefly mention the idea behind the EBOM and review the formulas needed in the present calculation. For more details we refer to Refs. 9 and 12.

The EBOM is a tight-binding-like model with the interaction parameters determined by requiring the model to predict the experimentally observed bulk band structure close to band edges. The model, which may be regarded as a discretized version of effective-mass theory, is particularly useful for describing electronic states in semiconductor heterostructures. Both ZnSe and $Zn_xMn_{1-x}Se$ (for the values of x encountered here) have a zinc-blende structure[13] with a basis containing two atoms located at the sites of the face-centered-cubic lattice. In a large-gap material like ZnSe [$E_g \simeq 2.8$ eV (Ref. 13)] a bond-orbital model which includes valence bands only, is sufficient. In this context a bond orbital is defined as the proper linear combination of atomic orbitals which best describes the states near the center of the Brillouin zone. We use the notation $|\mathbf{R},\alpha>$ for an α-like ($\alpha = x,y,z$) bond orbital located at a site $\mathbf{R}$ in the fcc lattice. The bond orbitals are assumed orthonormal, i.e., $<\mathbf{R}',\alpha'|\mathbf{R},\alpha>=\delta_{R,R'}\delta_{\alpha,\alpha'}$, and sufficiently localized so that only nearest-neighbor interactions have to be taken into account. The general form of the nearest-neighbor (and on-site) interactions are[9]

$$<\mathbf{R},\alpha|\,H\,|\mathbf{R}',\alpha'>=E_p\delta_{R,R'}\delta_{\alpha,\alpha'}+\sum_{\tau}\delta_{R'-R,\tau}\{E_{xy}\tau_\alpha\tau_{\alpha'}(1-\delta_{\alpha,\alpha'})+[E_{xx}\tau_\alpha^2+E_{zz}(1-\tau_\alpha^2)]\delta_{\alpha,\alpha'}\}, \tag{9}$$

where $E_{\alpha,\alpha'}$ is the interaction between an α-like orbital and an α'-like orbital located at the origin and at (1,1,0)$a/2$, respectively. E_p, E_{xx}, E_{xy}, and E_{zz} are four independent interaction parameters, and the sum over $\boldsymbol{\tau}$ covers the 12 nearest-neighbor position vectors. τ_α denotes the α component of $\boldsymbol{\tau}$ in units of $a/2$. The independent interaction parameters are determined by expanding the tight-binding Hamiltonian, $H(\mathbf{k})$, based on Eq. (9), to second order in $\mathbf{k}$ and requiring equivalence with multiband effective-mass theory. This scheme is thoroughly discussed in Ref. 9, and we merely quote the results. In terms of the Luttinger parameters γ_1, γ_2, and γ_3 the interaction parameters are found to be

$$E_{xy}=6\gamma_3\mathcal{R}_0,\quad E_{xx}=(\gamma_1+4\gamma_2)\mathcal{R}_0,$$
$$E_{zz}=(\gamma_1-8\gamma_2)\mathcal{R}_0,\quad E_p=E_v-12\gamma_1\mathcal{R}_0. \tag{10}$$

Here $\mathcal{R}_0\equiv\hbar^2/(2ma^2)$ and E_v denotes the band edge of the heavy-hole and light-hole valence bands. Since the Luttinger parameters are material dependent, the interaction parameters are in principle different in the well and barrier materials. In the present application, however, the Luttinger parameters γ_1,γ_2, and γ_3 for the barrier material $Zn_xMn_{1-x}Se$ are not known, and we assume the ZnSe values for these. In an unstrained quantum well the confining well potential comes in only through the position dependence of E_v in the last equation in (10).

The short-range hole-attractive potential from the isoelectronic trap is assumed to be nonzero only at the impurity site which is chosen as the origin,[14] i.e.,

$$<\mathbf{R}',\alpha'|V(\mathbf{r}_h)|\mathbf{R},\alpha>=-V_0\,\delta_{R,0}\delta_{R',0}\delta_{\alpha,\alpha'}\,, \tag{11}$$

where V_0 is an unknown parameter. Hole-attractive impurities correspond to negative values of V_0. V_0 is determined by fitting experimental data for the bound-exciton binding energy. All lattice relaxation effects are thus incorporated in the value of the single parameter V_0.

The large spin-orbit coupling of ZnSe, $\Delta = 0.45$ eV,[15] is exploited to reduce the size of the problem. The quantum well has the symmetry of the point group D_{2d}, and a Te impurity in the center does not alter this. In D_{2d} the p-like valence orbitals transform according to the Γ_4 and Γ_5 representations, while the electron spin ($s=\frac{1}{2}$) transforms as Γ_6. According to group theory $(\Gamma_4+\Gamma_5)\times\Gamma_6=\Gamma_6+{}^1\Gamma_7+{}^2\Gamma_7$. The p-like bond orbitals and the electron spin thus combine to a Γ_6-like and two different Γ_7-like pairs of spin-orbit-coupled bond orbitals (SOBO's). The Γ_7-like pairs can, however, be decomposed into two pairs of SOBO's where one of which is lifted with the energy Δ compared to the other. As an approximation we only include the energetically favored pair in our calculations, and this corresponds to neglecting the coupling to the split-off band. Using the Koster-Dimmock-Wheeler-Statz convention[16] we have the following SOBO's:

$$
\begin{aligned}
|\mathbf{R}, u^{\Gamma_6}_{1/2}> &= \frac{i}{\sqrt{2}}|\mathbf{R}, x> \phi^{\Gamma_6}_{-1/2} + \frac{1}{\sqrt{2}}|\mathbf{R}, y> \phi^{\Gamma_6}_{-1/2}, \\
|\mathbf{R}, u^{\Gamma_6}_{-1/2}> &= \frac{i}{\sqrt{2}}|\mathbf{R}, x> \phi^{\Gamma_6}_{1/2} - \frac{1}{\sqrt{2}}|\mathbf{R}, y> \phi^{\Gamma_6}_{1/2}, \\
|\mathbf{R}, u^{\Gamma_7}_{1/2}> &= -\frac{i}{\sqrt{6}}|\mathbf{R}, x> \phi^{\Gamma_6}_{-1/2} \\
&\quad + \frac{1}{\sqrt{6}}|\mathbf{R}, y> \phi^{\Gamma_6}_{-1/2} + i\frac{2}{\sqrt{6}}|\mathbf{R}, z> \phi^{\Gamma_6}_{1/2}, \\
|\mathbf{R}, u^{\Gamma_7}_{-1/2}> &= \frac{i}{\sqrt{6}}|\mathbf{R}, x> \phi^{\Gamma_6}_{1/2} \\
&\quad + \frac{1}{\sqrt{6}}|\mathbf{R}, y> \phi^{\Gamma_6}_{1/2} + i\frac{2}{\sqrt{6}}|\mathbf{R}, z> \phi^{\Gamma_6}_{-1/2},
\end{aligned}
\tag{12}
$$

where ϕ^{Γ_6} denotes the electron spinor. The Γ_6 (Γ_7) SOBO's are equivalent to heavy-hole (light-hole) SOBO's in bulk (see, e.g., Ref. 17) and are thus said to be heavy-hole-like (light-hole-like).

Optical studies of undoped ZnSe-$Zn_xMn_{1-x}Se$ quantum wells have revealed that the system is highly strained.[13,18,19] The effect of strain is readily incorporated in our EBOM formalism by adding a strain Hamiltonian H_{strain}, and the EBOM has already been used in band-structure calculations for strained $In_{1-x}Ga_xAs$-InP quantum wells.[20] From deformation potential theory we have the following:[20]

$$
\begin{aligned}
&< \mathbf{R}', u^{\Gamma_6}_{m'}|H_{\text{strain}}|\mathbf{R}, u^{\Gamma_6}_{m}> = (-\Delta V_H + D)\delta_{R,R'}\delta_{m,m'}, \\
&< \mathbf{R}', u^{\Gamma_7}_{m'}|H_{\text{strain}}|\mathbf{R}, u^{\Gamma_7}_{m}> = (-\Delta V_H - D)\delta_{R,R'}\delta_{m,m'}
\end{aligned}
\tag{13}
$$

where

$$\Delta V_H = 2(a_1 + a_2)(1 - C_{12}/C_{11})\epsilon_{\|} \tag{14}$$

and

$$D = b(2C_{12}/C_{11} + 1)\epsilon_{\|}. \tag{15}$$

Here C_{11} and C_{12} are elastic constants while a_1, a_2, and b are deformation potentials. The biaxial strain is given by $\epsilon_{\|} = (a_s - a_u)/a_u$ where a_u is the unstrained lattice constant (bulk) and a_s is the lattice constant in the plane of the heterointerface after accommodation of strain. The well material ZnSe has a smaller lattice constant in bulk than the barrier material $Zn_xMn_{1-x}Se$,[21] and $\epsilon_{\|}$ is thus positive in the well. Since the deformation potential b is a negative quantity[22] (and C_{11} and C_{12} are positive), D will be negative. Thus the light-hole-like valence states in the well will be higher in energy compared to the heavy-hole-like valence states. This splitting is reflected in results from photoluminescence experiments on certain ZnSe-$Zn_xMn_{1-x}Se$ superlattices where the light-hole free exciton is observed to be lower in energy than the corresponding heavy-hole exciton.[13] The influence of ΔV_H is merely to shift the energy gap and barrier height. The valence-band offsets for the present system are not accurately known, but they seem to be small and dominated by contributions from the lattice mismatch strain.[8] We will return to our choices for ΔV_H and D in Sec. IV.

The SOBO's in Eq. (12) could now in principle be used as basis functions in a variational calculation, but by further exploitation of symmetry a large reduction of the size of the computation can be achieved. According to group theory the localized hole states split into two symmetry types: Γ_7-like (light hole) and Γ_6-like (heavy hole). States of different symmetries are decoupled and can be treated independently. An appropriate set of angular functions to use as basis functions for $\Gamma_7^{-1/2}$-like states with even-parity envelopes is[12]

$$
\begin{aligned}
|\psi^{\Gamma_7}_{-1/2}(\mathbf{R})>_a &= |\mathbf{R}, u^{\Gamma_7}_{-1/2}>, \\
|\psi^{\Gamma_7}_{-1/2}(\mathbf{R})>_b &= \frac{Z^2 - \frac{1}{2}(X^2+Y^2)}{R^2}|\mathbf{R}, u^{\Gamma_7}_{-1/2}>, \\
|\psi^{\Gamma_7}_{-1/2}(\mathbf{R})>_c &= \frac{\sqrt{3}}{2}\frac{X^2 - Y^2}{R^2}|\mathbf{R}, u^{\Gamma_6}_{-1/2}>, \\
|\psi^{\Gamma_7}_{-1/2}(\mathbf{R})>_d &= \frac{iXY}{R^2}|\mathbf{R}, u^{\Gamma_6}_{-1/2}>, \\
|\psi^{\Gamma_7}_{-1/2}(\mathbf{R})>_e &= \frac{1}{\sqrt{2}}\frac{iYZ + XZ}{R^2}|\mathbf{R}, u^{\Gamma_6}_{1/2}>.
\end{aligned}
\tag{16}
$$

Here the z direction is defined as the growth direction, i.e., normal to material interfaces, X, Y, and Z are the components of $\mathbf{R}$, and $R^2 = |\mathbf{R}|^2 = X^2 + Y^2 + Z^2$. In Ref. 12 an additional angular basis function was included in the basis set, but in the present application this basis function turns out to be superfluous. Similarly, the necessary angular functions for $\Gamma_6^{1/2}$-like states are found to be

$$
\begin{aligned}
|\psi^{\Gamma_6}_{1/2}(\mathbf{R})>_a &= |\mathbf{R}, u^{\Gamma_6}_{1/2}>, \\
|\psi^{\Gamma_6}_{1/2}(\mathbf{R})>_b &= \frac{Z^2 - \frac{1}{2}(X^2+Y^2)}{R^2}|\mathbf{R}, u^{\Gamma_6}_{1/2}>, \\
|\psi^{\Gamma_6}_{1/2}(\mathbf{R})>_c &= \frac{\sqrt{3}}{2}\frac{X^2 - Y^2}{R^2}|\mathbf{R}, u^{\Gamma_7}_{1/2}>, \\
|\psi^{\Gamma_6}_{1/2}(\mathbf{R})>_d &= -\frac{iXY}{R^2}|\mathbf{R}, u^{\Gamma_7}_{1/2}>, \\
|\psi^{\Gamma_6}_{1/2}(\mathbf{R})>_e &= \frac{1}{\sqrt{2}}\frac{iYZ - XZ}{R^2}|\mathbf{R}, u^{\Gamma_7}_{-1/2}>.
\end{aligned}
\tag{17}
$$

(For definiteness we focus on the $\Gamma_7^{-1/2}$ and $\Gamma_6^{1/2}$ states of the Kramers-degenerate Γ_6-like and Γ_7-like pairs.)

In the calculations we use a cylindrical cluster of sites in the fcc lattice with the cylinder axis set in the growth direction. The angular functions in Eqs. (16) and (17) are combined with radial exponentials to give basis functions of the form

$$
\begin{aligned}
|\psi^{\Gamma}_{i}> = \sum_{\mathbf{R}} &\cos\left(\frac{\pi}{2}\frac{Z}{Z_{\text{cluster}}}\right)\cos\left(\frac{\pi}{2}\frac{\sqrt{X^2+Y^2}}{R_{\text{cluster}}}\right) \\
&\times e^{-\alpha_i\sqrt{X^2+Y^2+\mu_i Z^2}}|\psi^{\Gamma}_{m_i}(\mathbf{R})>,
\end{aligned}
\tag{18}
$$

where $2Z_{\text{cluster}}$ and R_{cluster} are the height and radius of the cluster, respectively, and the slowly varying cosine factors are included to tame an artificial discontinuity in the hole wave function at the cluster boundary. The sum

over $\mathbf{R}$ does not include the impurity site. The impurity-site bond orbital with the proper symmetry is included separately in the set of basis functions. Seven appropriately chosen α's and anisotropy parameters μ are used in the calculations to give a total of 36 basis functions. The interested reader is referred to Ref. 12 for information about how the calculation of the hole matrix elements is efficiently implemented on a computer.

B. Electrons

The conduction band of ZnSe has its minimum at the zone center, and a simple spherical effective-mass approximation including a quantum-well potential gives an adequate description. We thus use the Hamiltonian

$$H_e = -\frac{\hbar^2}{2m_e}\nabla_e^2 + V_{\mathrm{QW}}(z), \tag{19}$$

where m_e is the spherical effective mass and

$$V_{\mathrm{QW}}(z) = \begin{cases} 0 & \text{for } |z| < L/2 \\ V_{\mathrm{QW}}^C & \text{for } |z| \geq L/2. \end{cases} \tag{20}$$

Since the effective mass m_e for the barrier alloy is unknown, we assume for simplicity the well value throughout the heterostructure.

The quantum-well potential $V_{\mathrm{QW}}(z)$ includes both offset due to differences in band gap for unstrained materials and offset due to strain. The effect of strain on the conduction-band states is given in standard deformation potential theory as[20]

$$\Delta V_C = 2c_1(1 - C_{12}/C_{11})\epsilon_{\|}, \tag{21}$$

where c_1 is a deformation potential, C_{11} and C_{12} are elastic constants, and $\epsilon_{\|}$ is defined in the previous subsection. The strain will thus modify the barrier height from the "unstrained" value with the difference between the barrier and well value of ΔV_C. We shall return in Sec. IV to the choice of V_{QW}^C in our calculations.

For analytical convenience we use as basis functions in the variational calculations spherical harmonics Y_{lm} multiplied with Gaussians, i.e.,

$$\psi_e^{i,l_i}(\mathbf{r}) = \frac{1}{a^{*3/2}}\left(\frac{r}{a^*}\right)^{l_i} e^{-\beta_i r^2/a^{*2}}\, Y_{l_i m_i}(\theta,\phi)\,, \tag{22}$$

where a^* is the effective Bohr radius for the electron. We are interested in the ground state where the contribution from the s-like spherical harmonic Y_{00} is dominant. The present model has inversion symmetry around the impurity site in the middle of the well, and parity is thus a good quantum number. Therefore only even-parity spherical harmonics couple to Y_{00}. To ease the numerical calculation we restrict ourselves to s ($l = 0$) and d ($l = 2$) spherical harmonics in the basis. The kinetic term in Eq. (19) does not couple different spherical harmonics, and the only spherical harmonic of d-type which is coupled to Y_{00} via the quantum-well potential is Y_{20}.[23] Thus only two spherical harmonics, Y_{00} and Y_{20}, are included in the set of basis functions. The evaluation of the matrix elements

$$\begin{aligned} <\psi_e^{i,l_i}|H_e|\psi_e^{j,l_j}> &= \left\langle \psi_e^{i,l_i}\left|\left(-\frac{\hbar^2\nabla^2}{2m_e} + V_{\mathrm{QW}}(z)\right)\right|\psi_e^{j,l_j}\right\rangle \\ &\equiv \int d^3\mathbf{r}\,\frac{1}{a^{*3}}\left(\frac{r}{a^*}\right)^{l_i} e^{-\beta_i r^2/a^{*2}} Y_{l_i,0}\left(-\frac{\hbar^2}{2m_e}\nabla^2 + V_{\mathrm{QW}}(z)\right)\left(\frac{r}{a^*}\right)^{l_j} e^{-\beta_j r^2/a^{*2}} Y_{l_j,0} \end{aligned} \tag{23}$$

and overlaps

$$<\psi_e^{i,l_i}|\psi_e^{j,l_j}> \equiv \int d^3\mathbf{r}\,\frac{1}{a^{*3}}\left(\frac{r}{a^*}\right)^{l_i+l_j} \times e^{-(\beta_i+\beta_j)r^2/a^{*2}} Y_{l_i,0} Y_{l_j,0} \tag{24}$$

needed in the variational calulations is straightforward but tedious, and we refer the reader to Appendix A for the resulting expressions. Seven different β's are used in the calculations to give a total of $2 \times 7 = 14$ electron basis functions.

To check the flexibility of the present set of basis functions, we applied the set in a variational calculation on donor states in a quantum well. The resulting energies were compared with results from a study involving different trial wave functions by Oliveira[24] for parameters which resemble the current quantum-well system. The deviations in the predicted binding energies were found to be typically 0–2% which is accurate enough for the present application.

C. Electron-hole interaction

The mutual electron-hole interaction is modeled as a statically screened Coulomb interaction, namely,

$$v(|\mathbf{r}_h - \mathbf{r}_e|) = -\frac{e^2}{\epsilon_0|\mathbf{r}_h - \mathbf{r}_e|}, \tag{25}$$

where ϵ_0 is the static dielectric constant.

With the electron wave function given, the evaluation of V_{eff}^e in Eq. (5) is in principle straightforward. The electron wave function is represented by a linear combination of basis functions, i.e., $\psi_e = \sum_i C_i \psi_e^{i,l_i}$, where ψ_e^{i,l_i} is of the form shown in Eq. (22). The set of C_i's is output from the previous solution of the electron equation [Eq. (6)] in

the iteration scheme. With a normalized electron wave function as input, one has from Eqs. (5), (22), and (25)

$$V^e_{\rm eff}(\mathbf{r}_h) = < \psi_e(\mathbf{r}_e)|v(|\mathbf{r}_h - \mathbf{r}_e|)|\psi_e(\mathbf{r}_e) > = -\frac{e^2}{\epsilon_0 a^*}\sum_{i,j} C_i^* C_j \, V_{ij}(\mathbf{r}_h), \tag{26}$$

where

$$V_{ij}(\mathbf{r}_h) \equiv \left\langle \psi_e^{i,l_i} \left| \frac{a^*}{|\mathbf{r}_e - \mathbf{r}_h|} \right| \psi_e^{j,l_j} \right\rangle = \int d^3\mathbf{u} \, \frac{e^{-(\beta_i+\beta_j)u^2}}{|\mathbf{u} - \mathbf{r}_h/a^*|} Y^*_{l_i,0} Y_{l_j,0}. \tag{27}$$

In order to obtain numerically tractable expressions for $V_{ij}(\mathbf{r}_h)$, the factor $|\mathbf{u} - \mathbf{r}_h/a^*|^{-1}$ is expanded in a sum of spherical harmonics. For details about the evaluation of (27) we refer to Appendix B. With $V^e_{\rm eff}(\mathbf{r}_h)$ given and by applying the following simplification

$$< \mathbf{R}, \alpha|V^e_{\rm eff}(\mathbf{r}_h)|\mathbf{R}', \alpha' >= V^e_{\rm eff}(\mathbf{R})\delta_{R,R'}\delta_{\alpha,\alpha'} \ , \tag{28}$$

the matrix elements for the Coulomb interaction in Eq. (4) can be calculated. For the approximations involved in Eq. (28) to be valid, $V^e_{\rm eff}(\mathbf{r}_h)$ should be slowly varying on the scale of the lattice constant. This is presumably well fulfilled for the relatively extended electron wave functions encountered in the present calculation ($a^* \sim 29$ Å in ZnSe).

The analogous expression for $V^h_{\rm eff}(\mathbf{r}_e)$ to use in the electron equation [Eq. (6)] is obtained in a similar way. The hole wave function is given as a linear combination of basis functions,

$$|\psi_h >= \sum_i D_i |\psi_i^\Gamma > , \tag{29}$$

where $|\psi_i^\Gamma >$ is either of the form shown in Eq. (18) or a single bond orbital located at the impurity site. The set of D_i's is output from the previous solution of the hole equation [Eq. (4)]. This wave function may be written as a sum over individual SOBO's,

$$|\psi_h >= \sum_{\mathbf{R},j} G_j(\mathbf{R})|\mathbf{R}, u^{\Gamma_j}_{m_j} > , \tag{30}$$

where Γ_j is Γ_6 or Γ_7 and $m_j = \pm\frac{1}{2}$. This gives the following expression for the normalization constant:

$$< \psi_h|\psi_h >= \sum_{\mathbf{R},j} |G_j(\mathbf{R})|^2 = \sum_{\mathbf{R}} F(\mathbf{R}) \ . \tag{31}$$

$F(\mathbf{R})$ describes the probability for the hole to be at site $\mathbf{R}$. A natural approximation for the probability density $P(\mathbf{r}_h)$ is thus

$$P(\mathbf{r}_h) = \sum_{\mathbf{R}} F(\mathbf{R})\delta(\mathbf{R} - \mathbf{r}_h) \ . \tag{32}$$

With a normalized hole wave function, i.e.,

$$\int d^3\mathbf{r}_h \, P(\mathbf{r}_h) = \sum_{\mathbf{R}} F(\mathbf{R}) = 1 \ , \tag{33}$$

we find

$$V^h_{\rm eff}(\mathbf{r}_e) = -\frac{e^2}{\epsilon_0}\sum_{\mathbf{R}} \frac{F(\mathbf{R})}{|\mathbf{r}_e - \mathbf{R}|} \ . \tag{34}$$

The matrix elements to be used in the electron equation are then found to be

$$< \psi_e^{i,l_i}|V^h_{\rm eff}(\mathbf{r}_e)|\psi_e^{j,l_j} >= -\frac{e^2}{\epsilon_0 a^*}\sum_{\mathbf{R}} F(\mathbf{R})V_{ij}(\mathbf{R}), \tag{35}$$

where the sum naturally includes all sites in the cluster. In the evaluation of $V^h_{\rm eff}$ we treat a hole in a bond orbital centered at $\mathbf{R}$ as a point charge there. Also this approximation is justified by the reasonably large extension of the electron wave function.

Note that the presence of the electron-hole interaction, as it is included in the present calculational scheme, does not break the symmetry which underlies the symmetry-induced simplifications of the variational calculational scheme. Since $F(\mathbf{R})$ has quantum-well symmetry,[25] the only spherical harmonic coupled to Y_{00} via $V^h_{\rm eff}$ is Y_{20}.[23] Vice versa, with only Y_{00} and Y_{20} included in the electron basis, $V^e_{\rm eff}(\mathbf{r}_h)$ has quantum-well symmetry and does not reduce the symmetry of the pure hole Hamiltonian.

D. Bound-exciton calculations

Sections II A–II C contain recipes for calculations of all matrix elements needed to pursue the iterative scheme outlined in the beginning of the theory section. In practice the scheme is initiated by minimizing E_h in (4) in the absence of an electron, i.e., $V^e_{\rm eff} = 0$. Afterwards, the resulting hole wave function is used as input in the electron equation (6), whose output in turn is used as input for a new execution of the hole part. This loop is then repeated until the predictions for the energies have converged to within a preset tolerance. Typically four or five repetitions are sufficient.

In addition to predicting energies, we use the resulting (normalized) wave functions to calculate expectation values for the electron and hole distances from the impurity, i.e.,

$$< |\mathbf{r}_h| >= \sum_{\mathbf{R}} F(\mathbf{R})|\mathbf{R}| \ , \tag{36}$$

$$< |\mathbf{r}_e| >= \int d^3\mathbf{r}_e |\psi_e(\mathbf{r}_e)|^2 \, |\mathbf{r}_e| \ . \tag{37}$$

Our study also includes calculation of oscillator strengths for the bound exciton. The oscillator strength of a radiative transition for light with polarization $\mathbf{e}_x$, say, is[26]

$$f_x = \frac{2}{mE_0}| < f|\mathbf{e}_x \cdot \mathbf{p}|i > |^2 \ , \tag{38}$$

where E_0 is the energy of the transition, $\mathbf{p}$ is the momentum operator, and $|i >$ and $|f >$ represent the initial and final states, respectively. Within the effective-mass formalism the oscillator strength for the bound exciton has the form[27]

$$f_x = \frac{2}{mE_0} \sum_j | < u_{c0}|p_x|u^j_{v0} > |^2 \left| \int d^3\mathbf{r}\, \psi_e(\mathbf{r})\psi^j_h(\mathbf{r}) \right|^2 \tag{39}$$

when a separable wave function for the bound exciton, i.e.,

$$\Psi(\mathbf{r}_e, \mathbf{r}_h) = \left(\sum_j \psi^j_h(\mathbf{r}_h) u^j_{v0}(\mathbf{r}_h) \right) \psi_e(\mathbf{r}_e) u_{c0}(\mathbf{r}_e) \,, \tag{40}$$

is assumed. Here u_{c0} is the Γ-point conduction-band Bloch function in bulk, u^j_{v0} denotes a Γ-point valence-band Bloch function with the same symmetry as the SOBO $|\mathbf{R}, u^{\Gamma_j}_{m_j}>$, and ψ_e and ψ^j_h are envelope functions. Since we use EBOM to describe the holes, Eq. (39) must be modified correspondingly. In Appendix C it is shown that the appropriate expression for the oscillator strength for a j-like (Γ_6 or Γ_7) bound exciton is

$$f^j_x = \frac{2}{mE_0} | < u_{c0}|p_x|u^j_{v0} > |^2 V_\Omega \left| \sum_{\mathbf{R}} G_j(\mathbf{R})\psi_e(\mathbf{R}) \right|^2 \,, \tag{41}$$

where V_Ω is the volume of the primitive cell. The quantity $| < u_{c0}|p_x|u^j_{v0} > |^2$ is given in terms of the Kane matrix element E_K. Examination of the symmetry of the Bloch functions u^j_{v0} shows that $| < u_{c0}|p_x|u^j_{v0} > |^2$ equals $\frac{1}{12}mE_K$ for light holes (Γ_7) and $\frac{1}{4}mE_K$ for heavy holes (Γ_6), respectively.[28] The final expression for the oscillator strength for light polarized in the x direction is thus

$$f^j_x = c_j \frac{1}{2}\frac{E_K}{E_0} V_\Omega \left| \sum_{\mathbf{R}} G_j(\mathbf{R})\psi_e(\mathbf{R}) \right|^2 \,, \tag{42}$$

where $c_j = \frac{1}{3}$ for light-hole bound excitons and $c_j = 1$ for heavy-hole bound excitons.

III. BOUND EXCITONS IN BULK ZnSe

In this section we focus on bound excitons in *bulk* ZnSe. For the material parameters we use $a = 5.67$ Å for the lattice constant,[21] $\epsilon_0 = 8.66$ for the static dielectric constant,[29] $m_e = 0.16m_0$ for the electron effective mass,[15] and $\gamma_1 = 3.77, \gamma_2 = 1.24$, and $\gamma_3 = 1.67$ for the Luttinger parameters.[30] This parameter choice gives a bulk exciton binding energy of $\sim$ 20 meV,[31] in good agreement with experimental values.[15] To avoid finite-size effects on the hole wave function clusters involving up to 1.3×10^5 sites are used in the calculations. A small finite-size effect, however, will mainly affect the absolute values of the energies and not the energy difference between a bound exciton and a bound hole. Since V_0 is fitted to predict the experimentally observed energy for the bound exciton, the predicted value for the bound hole is rather insensitive to a small finite-size effect.

In zinc-blende structures the bulk ground state of the hole bound to a localized potential has Γ_8 symmetry with fourfold degeneracy (two heavy-hole states and two light-hole states). The four ground-state wave functions are not identical, however, and the heavy-hole and light-hole states have different spatial distributions of the hole density. Even within our present calculational scheme in which the electron-hole exchange interaction is omitted, the different hole densities couple differently with the electron to give an energy splitting between heavy-hole-like and light-hole-like bound excitons in bulk. This energy splitting is observed to be very small, however, and within the accuracy of our calculational scheme we find the heavy-hole-like and light-hole-like bound excitons to have the same energy.

The d-like members of the electron basis functions are found to be essentially decoupled from the dominant s-like part and can, as a good approximation, be left out of the basis in the bulk case.

In Fig. 1 we show the ground-state energies for a bound exciton and a bound hole, respectively, as functions of the depth of the isoelectronic potential V_0. The dominating peak in the photoluminescence spectra for bulk ZnSe:Te has its maximum located 120 meV below the free-exciton peak.[3,7] Given that the interpretation in Refs. 7 and 8 is correct, namely, that the peak is due to recombination of excitons bound to single Te impurities, the value of V_0 corresponding to this physical situation is $V_0 = -2640$ meV. For this value of V_0, marked with a vertical dotted line in Fig. 1, a bound hole alone has 27.7 meV higher energy than the bound exciton. Since the lattice relaxation energy involved in the self-trapping of the hole presumably is not much affected by the presence or absence of the electron, one can assume the same value of V_0 for the bound hole as for the bound exciton. With a free exciton binding energy of 20 meV, a bound-hole level at ~ -112 meV is thus predicted in ZnSe:Te. As we mentioned in

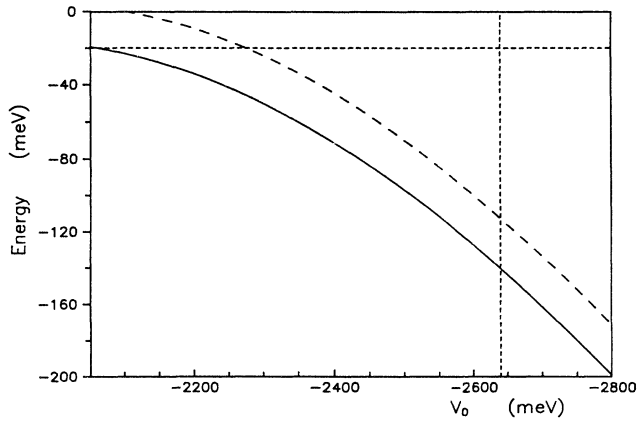

FIG. 1. Ground-state energies of a bound exciton (solid line) and a bound hole + a free electron (dashed line) localized at a single Te impurity in bulk ZnSe as functions of the depth of the isoelectronic impurity potential V_0. The zero of energy corresponds to a hole at the valence-band edge and an electron at the conduction-band edge in bulk ZnSe. The horizontal dotted line indicates the energy of the free exciton in ZnSe while the vertical dotted line at $V_0 = -2640$ meV represents the position of the dominant bound exciton peak in the photoluminescence spectra of dilute ZnSe:Te.

the Introduction, the question of the interpretation of the photoluminescence peaks is not fully settled. In Refs. 4 and 5 a smaller feature located 25 meV below the free-exciton peak was observed and interpreted as due to excitons bound to pairs of Te impurities. For completeness we briefly comment that this spectral feature corresponds energetically to an exciton bound to a single Te impurity with $V_0 = -2275$ meV.

The results in Fig. 1 also show that for such small values of $|V_0|$ that a hole does not bind, an exciton may still be more deeply bound than the 20 meV (Ref. 15) for a free exciton. For large negative values of V_0 the hole is deeply bound and strongly localized around the impurity site. In these cases the electron thus effectively sees a positively charged impurity, and the difference between the energies of the bound exciton and the bound hole is close to the effective-mass donor binding energy of 29.0 meV.[32]

The shrinkage of the hole wave function with increasing potential depth is illustrated in Fig. 2 where the mean distances from the impurity site for the electron and hole constituting the bound exciton are plotted. (Note that Figs. 2–4 contain results of both bulk and quantum-well calculations. The latter calculations are described in Sec. IV.) While the hole distance is seen to be small and continously decreasing with increasing $|V_0|$, the electron distance is much larger and slowly varying and approaches the effective-mass donor value of 43 Å (Ref. 32) in the large $|V_0|$ limit. For $V_0 = -2640$ meV, which corresponds to the dominating peak in the photoluminescence spectra for dilute $ZnTe_xSe_{1-x}$ ($x \simeq 0.01$), $< |\mathbf{r}_h| >$ is found to be 4.8 Å for the bound exciton. Note, however, that this is a slight underestimate. A substantial fraction of the hole charge density is located at the impurity site, and the contribution from this site to the averaging sum in Eq. (36) is, inaccurately, set to zero. An interesting feature is that $< |\mathbf{r}_h| >$ for the isolated bound hole

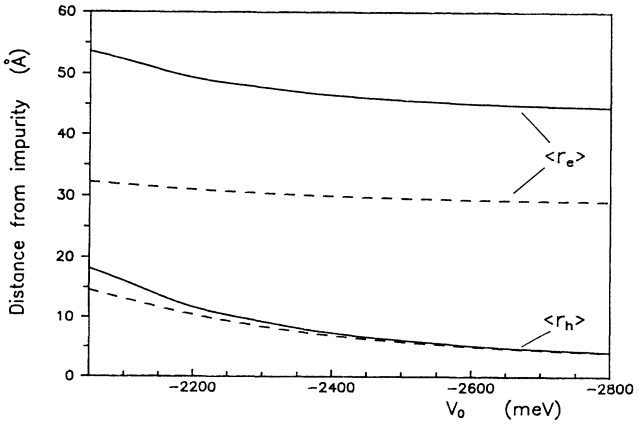

FIG. 2. Average distances from the Te impurity for the hole and electron in the bound exciton, as functions of the depth of the isoelectronic impurity potential V_0. The formulas are given in Eqs. (36) and (37). Solid curves represent excitons bound to single Te impurities in bulk ZnSe while dashed curves represent light-hole-like bound excitons localized at a single Te impurity centered in a 43-Å-wide ZnSe-$Zn_{0.79}Mn_{0.21}Se$ strained quantum well.

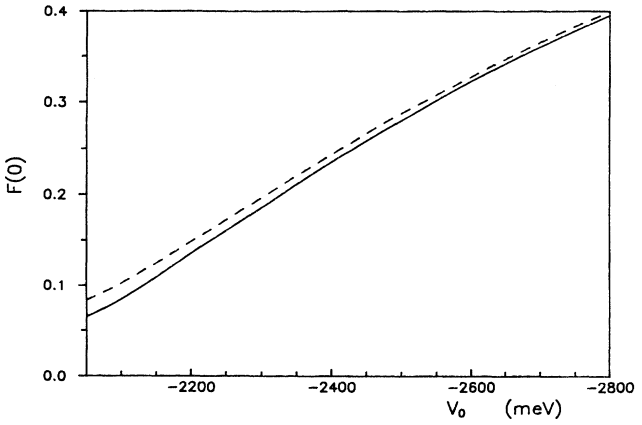

FIG. 3. Probability of finding the hole in the bound exciton at the impurity site, $F(0)$, as function of the depth of the isoelectronic impurity potential V_0. The solid curve represents excitons bound to single Te impurities in bulk ZnSe while the dashed curve represents light-hole-like bound excitons localized at a single Te impurity centered in a 43-Å-wide ZnSe-$Zn_{0.79}Mn_{0.21}Se$ strained quantum well.

for $V_0 = -2640$ meV is 4.9 Å, slightly larger than the bound-exciton value. This is an illustration of the extra binding of the hole in the bound exciton due to Coulomb interaction with the electron.

The strong localization of the hole is further illustrated in Fig. 3 where the probability of finding the hole in the bound exciton on the impurity site, $F(0)$, is plotted as function of V_0. For $V_0 = -2640$ meV we observe $F(0) = 0.34$.

The oscillator strength for a light-hole-like bound exciton for light polarized in the x direction, $f_x^{\Gamma_7}$, as function of V_0 is displayed in Fig. 4. The corresponding oscillator

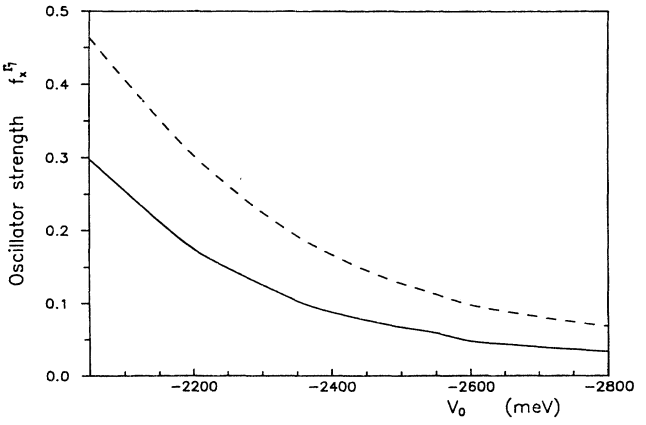

FIG. 4. Oscillator strengths of a light-hole-like bound exciton for light polarized in the x direction, $f_x^{\Gamma_7}$, as functions of the depth of the isoelectronic impurity potential V_0. The formula for $f_x^{\Gamma_7}$ is given in Eq. (42). The solid curve corresponds to excitons bound to single Te impurities in bulk ZnSe while the dashed curve represents bound excitons localized at a single Te impurity centered in a 43-Å-wide ZnSe-$Zn_{0.79}Mn_{0.21}Se$ strained quantum well. The small oscillations on the bulk curve are due to inaccuracies in our variational calculation and do not have a physical origin.

strength for the heavy-hole-like bound exciton, $f_x^{\Gamma_6}$, is a factor of 3 higher. For the Kane matrix element we use $E_K = 24.2$ meV.[30] We observe a decrease in the oscillator strength with the increase of $|V_0|$ (and thus increase of the hole binding). This is expected since the oscillator strength reflects the overlap between the electron and hole wave functions, which decreases when the difference in scale between the electron and hole wave functions increases.

IV. BOUND EXCITONS IN STRAINED QUANTUM WELLS

In this section we extend our study to strained ZnSe-$Zn_{1-x}Mn_xSe$ quantum wells with single Te impurities centered in the well. The main motivation for this is the recent experimental study of this system by Fu *et al.*[8] They performed optical measurements on 44-Å-wide ZnSe-$Zn_{1-x}Mn_xSe$ ($x \simeq 0.21$) quantum wells with a monolayer sheet of Te impurities incorporated in the center of the well. The monolayer of ZnTe is subject to both interdiffusion and strain. The lattice mismatch between ZnTe and ZnSe is very large, approximately 7%, but a defect-free epitaxial structure is still expected.[8] Two peaks, interpreted as due to recombination of bound excitons located at single Te atoms and pairs of Te atoms, respectively, were observed in the photoluminescence spectra. The dominance of these two peaks was explained by interdiffusion of Te atoms to make singles and pairs the most frequently occurring cluster species in the distribution of Te clusters. From magneto-optical measurements Fu *et al.* concluded that the bound-exciton hole wave function is strongly localized around the Te impurities while the electron is bound to the hole in a donorlike fashion. The strong localization of the hole around the Te impurities and the assignment of the two peaks to exciton localization at single and pairs of Te impurities, respectively, indicate that the single impurity case, as a first approximation, can be modeled by assuming one single Te impurity located at the center of the quantum well.

The band offsets and the energy splitting between light-hole-like and heavy-hole-like valence-band states are not precisely known for this system. Optical studies of $Zn_{0.77}Mn_{0.23}Se$ and ZnSe single-crystal films have revealed a total band-gap difference of 110 meV for the unstrained heterojunction for $x = 0.23$,[19] and we use this value for our structure with $x = 0.21$. A large strain modifies this value substantially and also causes a splitting of the light-hole and heavy-hole valence-band edges. The lattice constant for single-crystal $Zn_{1-x}Mn_xSe$ has been measured by Yoder-Short, Debska, and Furdyna.[21] For $x = 0.21$ they predict the lattice constant to be 0.85% larger than in the well material ZnSe. The barrier material thus imposes on the well material a tensile strain parallel to the interface and a compressive strain normal to the interface, and $\epsilon_{\parallel}$ is thus positive in the well. Since values for deformation potentials and elastic constants are known only for the well material ZnSe, we assume these values for the barrier material also. For the ratio between the elastic constants we use $C_{12}/C_{11} = 0.605$.[15] For the deformation potential b we use the experimental value -1.2 eV.[22] The deformation potentials a_1, a_2, and c_1 are not known individually, but the sum $(a_1+a_2+c_1)$, often called the hydrostatic deformation potential, is experimentally found to be -5.4 eV.[22] Therefore we cannot calculate ΔV_C and ΔV_H independently, only their sum. Since the well is much narrower than the barriers, which are typically 500 Å wide or more,[33] we further assume that *all* strain is accommodated in the well material. This means that the common in-plane lattice constant in the quantum-well structure is identical to the bulk lattice constant of the barrier material. (We shall come back to this point later.) With the present choice of material parameters we then have $D = -22$ meV and $\Delta V_C + \Delta V_H = -36$ meV in the well and zero in the barrier. Inspection of Eq. (13) shows that the light-hole-like band edge in the well is raised in energy in the presence of the strain. Thus the light-hole-like valence states become energetically favorable relative to the heavy-hole-like states in the well. Moreover, the band gap will be reduced. To specify the heterostructure completely we must choose a value for the light-hole-like valence band offset. Fu *et al.*[8] suggested $\Delta E_{\rm LH} \sim 30$ meV, based on previous optical studies of ZnSe-$Zn_{1-x}Mn_xSe$ quantum wells of similar layer thicknesses and Mn concentrations and found this value to be compatible with their own magneto-optical studies. The effect of strain can be incorporated in "effective" band edges for light holes and heavy holes, and with the choice of Fu *et al.* for $\Delta E_{\rm LH}$ these effective band edges are

$$E_{\rm LH}^{\rm well} = 0,\ E_{\rm LH}^{\rm barrier} = -30 \text{ meV},$$
$$E_{\rm HH}^{\rm well} = -44 \text{ meV},\ E_{\rm HH}^{\rm barrier} = -30 \text{ meV}. \tag{43}$$

The conduction-band offset follows from subtracting $\Delta E_{\rm LH}$ from the sum of the "unstrained" band gap, $|\Delta V_C + \Delta V_H|$, and $|D|$, and we find $V_{\rm QW}^C = 138$ meV. One notices that the system is predicted to be type II for the heavy holes. The band lineup is schematically illustrated in Fig. 5.

To check the correctness of this set of parameters, we

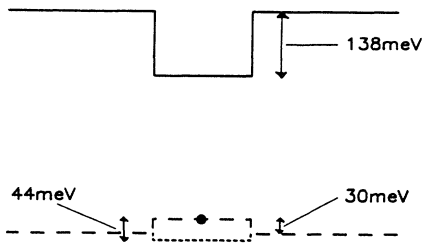

FIG. 5. Schematic illustration of the band lineup (in the electron convention) for the present quantum well structure according to (43). The dashed and dotted lines correspond to the light-hole and heavy-hole "effective" band edges, respectively, after accomodation of strain. The filled dot symbolizes the hole-attractive Te impurity.

investigated the implications on the energetical positions of the light-hole and heavy-hole free excitons and compared with experiments. The splitting between the type-I light-hole and type-II heavy-hole exciton was calculated using an extension of the multiband effective-mass formalism of Sanders and Chang[34] as modified by Wu and Nurmikko.[35] We discuss our method in Appendix D. We obtain 29.5 and 12.3 meV for the light-hole and heavy-hole exciton binding energies. Since the structure is type II for heavy holes, the electrons and holes are spatially confined in different regions. This significantly reduces the binding from the mutually attractive Coulomb potential. Even though the lowest heavy-hole single-particle state (−30 meV) is only 10 meV lower in energy than the lowest light-hole subband edge (−19.6 meV), the exciton splitting is found to be 27.6 meV with the parameter values above. This seems to be consistent with what is experimentally observed by Fu *et al.* In their photoluminescence excitation spectra a small and broad peak is observed at the high-energy side of the dominant exciton peak. Its size and shape support the interpretation that the peak is due to type-II heavy-hole excitons. In type-I structures the heavy-hole peaks are usually larger than the light-hole peak, but when the structure is type II for the heavy holes, the reduced electron and hole overlap may change this completely. Optical transitions involving spatially separated states also tends to have a smoothing effect on the spectra, and the identification of the onset energy for the transition is not always clear.[36] A rough value for the experimentally observed splitting between the light-hole and heavy-hole exciton is ~ 30–50 meV, somewhat higher than our theoretical value of 27.6 meV.

Competition between the strain-induced reduction of the light-hole energy gap and the confining well potential decides whether the light-hole free exciton is red-shifted or blue-shifted compared to free excitons in bulk ZnSe. The photoluminescence spectra at 6.5 K for a ZnSe epilayer exhibits a dominant free-exciton peak at ~ 2800 meV.[18] With a bulk exciton binding energy of 20 meV (Ref. 15) this gives at fundamental band gap, E_g, of 2820 meV in bulk ZnSe. To give an estimate of the position of the light-hole free-exciton peak in the present quantum-well structure, the electron and light-hole subband edges are needed. These energies follow from solving the standard "particle in a potential well" problem[37] which gives 45.3 meV for the electrons and 19.6 meV for the light holes $[m_{\mathrm{LH}}/m_0 = (\gamma_1 + 2\gamma_2)^{-1}]$ for the present 44-Å-wide quantum well. Using the scheme for calculating exciton energies described in Appendix D, a binding energy of 29.5 meV is predicted. With the previously listed values for D and $\Delta V_h + \Delta V_c$, this adds up to a light-hole exciton at 2797 meV. In the photoluminescence excitation spectra of Fu *et al.*,[8] measured at 2 K, the lowest peak, presumably due to the light-hole exciton, is located at ~ 2818 meV.

The 20-meV discrepancy may be due in part to uncertainty in the deformation potentials. The discrepancy between the theoretical and experimentally observed value for the predicted blue-shift of the free light-hole exciton can also to some extent be accounted for by assuming a smaller strain in the ZnSe well material, i.e., 70–80 % of the full strain. This would raise the strained ZnSe gap and thus the energy of the light-hole free exciton. Assuming the same in-plane lattice constant in the strained well and barrier materials, reduced tensile strain in the well will imply compressive strain in the barrier material. This will lower the predicted energy splitting between light-hole and heavy-hole excitons and make the agreement with experiment less good in this respect. At first glance it may seem that this can be remedied by assuming a larger value for ΔE_{LH}. The problem is that this would make the structure "less" type II for the heavy holes. This implies an increase of the heavy-hole exciton binding energy and thus a reduction of the predicted exciton splitting. However, if we assume the presence of nonuniform strain in the barrier or some free-carrier distribution (due to unintentional doping), then the resulting band bending may be sufficient to localize the heavy hole far away from the interface. Thus the exciton associated with the highest heavy-hole subband may become unobservable, and the observed high-energy exciton peak in Ref. 8 may be attributed to excitons stemming from unconfined heavy-hole subbands (which would be more localized in the ZnSe layer). Evidence for such "unconfined" excitons has been observed previously.[38] We suspect that the unidentified structure observed in Ref. 19 (the rightmost bump in the PLE spectrum of Fig. 1 of Ref. 19) is also due to excitons stemming from unconfined heavy-hole states. Despite the uncertainties mentioned here, our results for the bound excitons and the comparison with experiment would not be significantly altered by assuming a slightly different strain distribution.

In Fig. 6 we show energies of the light-hole-like bound-exciton ground states for a 43-Å-wide ZnSe-$Zn_{0.79}Mn_{0.21}Se$ quantum well with a centered Te impurity as function of V_0. This well width corresponds to 15 atomic layers in the well. The energy gap in (strained) ZnSe is chosen as the zero of energy. For comparison we also plot the energy of the corresponding bound hole plus the energy of a free electron at the lowest subband edge. The difference between this energy and the bound-exciton energy corresponds to the energy gained when an electron binds to an impurity-bound hole. To compare our results for the bound exciton with experiment, the energy of the light-hole exciton is needed. Using the scheme in Appendix D an energy of 37 meV is found, and this energy is also marked in Fig. 6. The dominating bound-exciton peak in bulk spectra with an energy 120 meV less than the free-exciton peak, is seen in Ref. 8 to be 100 meV below the free-exciton peak in the spectra for the present quantum well. This bound-exciton peak must be due to recombination of the light-hole-like bound exciton, and corresponds to $V_0 = -2530$ meV in Fig. 6. This value should be compared with $V_0 = -2640$ meV predicted by the bulk calculations. We will comment on possible reasons for this discrepancy in the next section.

For completeness we mention that the smaller feature observed 25 meV below the free-exciton peak in photoluminescence on bulk samples,[4,5] is seen to be 45 meV below the free exciton in the quantum-well spectra. This corresponds to $V_0 = -2315$ meV in Fig. 6, in good agree-

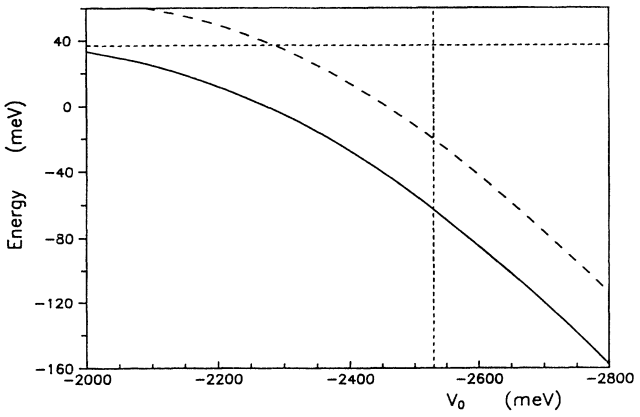

FIG. 6. The ground-state energies of a light-hole-like bound exciton (solid) and a light-hole-like bound hole + a free electron (dashed) localized at a single Te impurity centered in a 43-Å-wide ZnSe-$Zn_{0.79}Mn_{0.21}Se$ strained quantum well, as functions of the depth of the isoelectronic impurity potential V_0. The zero of energy corresponds to a hole at the light-hole bulk valence-band edge and an electron at the bulk conduction-band edge in ZnSe *after* accomodation of strain (as described in the main text). The horizontal dotted line indicates the energy of the light-hole-like quantum-confined free exciton in the quantum well. The vertical dotted line at $V_0 = -2530$ meV represents the position of the dominant bound-exciton peak in the photoluminescence spectra of Fu *et al.* (Ref. 8).

ment with the predicted value from the bulk calculations. The bulk value for V_0 ($V_0 = -2275$ meV) corresponds to a binding energy of 38 meV, i.e., 7 meV less than the experimental value.

The average electron and hole distances from the impurity, $< |\mathbf{r}_e| >$ and $< |\mathbf{r}_h| >$, for the light-hole-like bound exciton are plotted as functions of V_0 in Fig. 2. When comparing with the results for bulk, we observe that $< |\mathbf{r}_e| >$ is substantially reduced by the confining quantum-well potential which makes it energetically favorable for the electron to localize closer to the impurity in the middle of the well. The strongly localized hole wave function is much less affected by the presence of the barrier. For $V_0 = -2530$ meV, which is experimentally relevant, we find $< |\mathbf{r}_e| >= 29.6$ Å and $< |\mathbf{r}_h| >= 5.5$ Å.

In Fig. 3 the probability of finding the hole in the light-hole bound exciton at the impurity site, $F(0)$, is shown as function of V_0. We see that $F(0)$ is slightly increased when comparing with bulk results (for the same V_0), and this is mainly due to confinement by the valence-band well potential. The confinement of the electron by the quantum-well potential is also reflected in the enhancement of the oscillator strength as seen in Fig. 4.

A different choice for the light-hole valence-band offset does not alter our results significantly. For $V_0 = -2530$ meV less than 1% of the hole probability density is in the barrier material. By choosing, for example, $\Delta E_{\mathrm{LH}} = 44$ meV instead of 30 meV for this value of V_0, the energy of the bound light hole is shifted with 0.1 meV. The energy of the light-hole-like bound exciton is reduced with $\simeq 2$ meV due to the accompanying lowering of the well potential seen by the electron (from 138 to 124 meV).

We also calculated for $V_0 = -2530$ meV the energies of the heavy-hole-like (Γ_6) bound hole and bound exciton and found the binding to be reduced with 22 meV compared to the corresponding light-hole-like states. This difference is only one half of the difference between the light-hole and heavy-hole effective band edges in the well material (44 meV). This illustrates the substantial mixing of heavy-hole and light-hole SOBO's in the bound-hole and bound-exciton wave functions.

V. DISCUSSION AND CONCLUDING REMARKS

In the present work we have calculated properties of bound excitons in Te-doped bulk ZnSe and ZnSe-$Zn_{1-x}Mn_xSe$ strained quantum wells. The value of the hole-attractive potential V_0, which includes self-trapping effects, has been determined by fitting experimental values for the bound-exciton binding energy. A discrepancy between the fitted values of V_0 for the bulk case ($V_0 = -2640$ meV) and the quantum-well case ($V_0 = -2530$ meV) is observed, and possible reasons for this discrepancy are discussed below.

In our calculation we have studied binding to a single Te impurity in the middle of the quantum well, and not to a plane containing numerous Te impurities which is the experimental situation. Although the strong localization of the hole wave function around the single impurity suggests that these situations are not so different as far as binding of bound excitons is concerned, we are inclined to believe that this is the main reason for the observed discrepancy. Since the lattice mismatch between ZnTe and ZnSe is large, additional strain occurs in the region around the impurity sheet. In addition to introducing potential terms in the bound-exciton Hamiltonian, this strain will also modify the self-trapping and the accompanying lattice relaxation and therefore change the appropriate value to use for the impurity potential V_0.

Also the strain induced on the ZnSe well material by the $Zn_{1-x}Mn_xSe$ barriers may influence the hole self-trapping and thus effectively change the appropriate value to use for V_0. The results may also have been influenced by the uncertainty connected to the choice of material parameters, the accommodation of strain, and the approximations involved in the solution of the bound-exciton equations. However, since the bound exciton is localized around the impurity, one generally expects the confinement energy to be less for bound excitons than free excitons in a quantum well. Thus for all reasonable choices of confining potentials and deformation potentials the bound-exciton binding energy, i.e., the difference between the bound-exciton and free-exciton energy, will be larger in the quantum-well case than in the bulk case. Since the experimental results on the contrary show a 20-meV lower bound-exciton binding energy in the quantum well compared to bulk, we do not believe that these sources of inaccuracy account for a major part of the observed discrepancy.

The electron-hole exchange interaction is presumably

larger in the quantum well than in bulk because of the larger electron-hole overlap in the former case.[2] The approximation of neglecting exchange interactiom in the present calculational scheme is thus an error source which may account for some of the observed discrepancy in the values of V_0.

The strain induced on the the ZnSe well material by the $Zn_{1-x}Mn_xSe$ barriers may also influence the hole self-trapping and thus effectively change the appropriate value to use for V_0. Likewise, the results may have been influenced by the uncertainty connected to the choice of material parameters, the accommodation of strain, and the approximations involved in the solution of the bound-exciton equations. However, we do not believe that these effects can account for a substantial part of the observed discrepancy.

The strong localization of the hole wave function around the Te impurity for intermediate and large values of $|V_0|$ may raise a question about the applicability of the EBOM to this system. However, the previous success of EBOM in the description of acceptor states with similarly large binding energies and probabilities of finding the hole *on* the impurity site as in the present case,[39] indicates that the EBOM offers a reasonably accurate description.

To probe our conjecture for the reason for the observed discrepancy, we suggest an experiment in which single Te impurities in quantum wells can be studied unambiguously. This can be achieved through dilute doping of Te impurities in the central region of the quantum well so that strain effects due to the ZnTe monolayer and interactions between adjacent impurities are definitely avoided.

The calculated oscillator strengths in Fig. 4 will hopefully be used to calculate recombination lifetimes of the bound exciton to compare with experimental lifetime measurements, assuming that such will become available, to shed further light on the physics of these interesting systems.

ACKNOWLEDGMENTS

This work was supported in part by the U.S. Office of Naval Research under Contract No. N00014-89-J-1157 and by the University of Illinois Material Research Laboratory under Contract No. NSF-DMR-86-12860. We acknowledge the use of Cray X-MP/216 at RUNIT, University of Trondheim.

APPENDIX A

The form of the electron basis functions are shown in Eq. (22) where

$$Y_{00} = \sqrt{1/4\pi},$$
$$Y_{20} = \sqrt{5/16\pi}(3\cos^2\theta - 1) = \sqrt{5/16\pi}\frac{2z^2-(x^2+y^2)}{r^2}. \tag{A1}$$

The kinetic-energy operator does not couple Y_{00} and Y_{20}, and the matrix elements

$$\left\langle \psi_e^{i,l_i} \left| \left(-\frac{\hbar^2\nabla^2}{2m_e}\right) \right| \psi_e^{j,l_j} \right\rangle \equiv -\frac{\hbar^2}{2m_e}\int d^3\mathbf{r}\,\frac{1}{a^{*3}}\left(\frac{r}{a^*}\right)^{l_i} e^{-\beta_i r^2/a^{*2}} Y_{l_i 0}\,\nabla^2\,\left(\frac{r}{a^*}\right)^{l_j} e^{-\beta_j r^2/a^{*2}} Y_{l_j 0} \tag{A2}$$

are found to be

$$\left\langle \psi_e^{i,0} \left| \left(-\frac{\hbar^2\nabla^2}{2m_e}\right) \right| \psi_e^{j,0} \right\rangle = E^*_{Ry}[6\beta_j I(2,\beta_i+\beta_j) - 4\beta_j^2 I(4,\beta_i+\beta_j)],$$
$$\left\langle \psi_e^{i,2} \left| \left(-\frac{\hbar^2\nabla^2}{2m_e}\right) \right| \psi_e^{j,2} \right\rangle = E^*_{Ry}[14\beta_j I(6,\beta_i+\beta_j) - 4\beta_j^2 I(8,\beta_i+\beta_j)], \tag{A3}$$

where $E^*_{Ry} = \hbar^2/(2m_e a^{*2})$ and

$$I(n,\beta) \equiv \int_0^\infty du\, u^n e^{-\beta u^2} = \frac{1}{2}\,\beta^{-(n+1)/2}\,\Gamma\left(\frac{n+1}{2}\right). \tag{A4}$$

Here Γ denotes the Γ function.

Similarly the overlaps are found to be

$$< \psi_e^{i,l_i} | \psi_e^{j,l_j} > = I(2+l_i+l_j, \beta_i+\beta_j)\delta_{l_i,l_j}. \tag{A5}$$

The matrix elements from $V_{QW}(z)$ are slightly more cumbersome to evaluate and are obtained as follows:

$$< \psi_e^{i,0}|V_{\rm QW}(z)|\psi_e^{j,0} > = \frac{1}{\pi} I(0,\beta_i+\beta_j)^2 \int_{-\infty}^{\infty} du\, V_{\rm QW}(ua^*) e^{-(\beta_i+\beta_j)u^2},$$

$$< \psi_e^{i,0}|V_{\rm QW}(z)|\psi_e^{j,2} > = \frac{\sqrt{5}}{4\pi}\left(\frac{\pi}{\beta_i+\beta_j} \int_{-\infty}^{\infty} du\, u^2 V_{\rm QW}(ua^*) e^{-(\beta_i+\beta_j)u^2} - \sqrt{\pi/(\beta_i+\beta_j)} I(2,\beta_i+\beta_j) \int_{-\infty}^{\infty} du\, V_{\rm QW}(ua^*) e^{-(\beta_i+\beta_j)u^2} \right), \tag{A6}$$

$$< \psi_e^{i,2}|V_{\rm QW}(z)|\psi_e^{j,2} > = \frac{5}{16\pi}\left[4\frac{\pi}{\beta_i+\beta_j} \int_{-\infty}^{\infty} du\, u^4 V_{\rm QW}(ua^*) e^{-(\beta_i+\beta_j)u^2} - 8\sqrt{\pi/(\beta_i+\beta_j)} I(2,\beta_i+\beta_j) \int_{-\infty}^{\infty} du\, u^2 V_{\rm QW}(ua^*) e^{-(\beta_i+\beta_j)u^2} + \left(2\sqrt{\pi/(\beta_i+\beta_j)} I(4,\beta_i+\beta_j) + 2I(2,\beta_i+\beta_j)^2 \right) \int_{-\infty}^{\infty} du\, V_{\rm QW}(ua^*) e^{-(\beta_i+\beta_j)u^2} \right],$$

where

$$\int_{-\infty}^{\infty} du\, V_{\rm QW}(ua^*) e^{-\beta u^2} = V_{\rm QW}^C \sqrt{\pi/\beta}\, \{1 - \mathrm{erf}[L\sqrt{\beta}/(2a^*)]\},$$

$$\int_{-\infty}^{\infty} du\, u^2 V_{\rm QW}(ua^*) e^{-\beta u^2} = V_{\rm QW}^C \left(\frac{\sqrt{\pi}\beta^{-3/2}}{2} \{1 - \mathrm{erf}[L\sqrt{\beta}/(2a^*)]\} + \frac{L}{2a^*\beta} e^{-\beta L^2/(4a^{*2})} \right), \tag{A7}$$

$$\int_{-\infty}^{\infty} du\, u^4 V_{\rm QW}(ua^*) e^{-\beta u^2} = V_{\rm QW}^C \left[\frac{3\sqrt{\pi}\beta^{-5/2}}{4} \{1 - \mathrm{erf}[L\sqrt{\beta}/(2a^*)]\} + \left(\frac{3L}{4a^*\beta^2} + \frac{L^3}{8a^{*3}\beta} \right) e^{-\beta L^2/(4a^{*2})} \right],$$

and

$$\mathrm{erf}(x) \equiv \frac{2}{\sqrt{\pi}} \int_0^x du\, e^{-u^2}. \tag{A8}$$

APPENDIX B

To obtain a numerically tractable expression for $V_{ij}(\mathbf{R})$, defined in Eq. (27), we use the following standard expansion:[40]

$$\frac{1}{|\mathbf{u} - \mathbf{R}/a^*|} = 4\pi \sum_{l=0}^{\infty} \sum_{m=-l}^{l} \frac{1}{2l+1} \frac{u_<^l}{u_>^{l+1}} \times Y_{lm}(\Omega_u) Y_{lm}(\Omega_{\mathbf{R}}). \tag{B1}$$

Here $u_> = \max(|\mathbf{u}|, |\mathbf{R}|/a^*)$ and $u_< = \min(|\mathbf{u}|, |\mathbf{R}|/a^*)$, respectively. Insertion into Eq. (27) gives

$$V_{ij}(\mathbf{R}) = 4\pi \sum_{l=0}^{\infty} \frac{1}{2l+1} I_u(l, \beta_i+\beta_j, |\mathbf{R}|) \times \sum_{m=-l}^{l} Y_{lm}(\Omega_{\mathbf{R}}) I_\Omega(i, lm, j), \tag{B2}$$

where

$$I_u(l,\beta,|\mathbf{R}|) \equiv \int_0^{\infty} du\, \frac{u_<^l}{u_>^{l+1}} u^2 e^{-\beta u^2}, \tag{B3}$$

$$I_\Omega(i, lm, j) \equiv \int d\Omega\, Y_{i0}^* Y_{lm} Y_{j0}. \tag{B4}$$

The integral I_u is given in terms of incomplete Γ functions which are available as standard functions in numerical libraries. The integral I_Ω is given in terms of products of $3j$ symbols (see, for example, Ref. 41).

APPENDIX C

In the effective-mass approximation the oscillator strength for light polarized in the x direction is [see Eq. (39)]

$$f_x = \frac{2}{mE_0} \sum_j | < u_{c0}|p_x|u_{v0}^j > |^2 \times \left| \int d^3r\, \psi_h^j(\mathbf{r}) \psi_e(\mathbf{r}) \right|^2. \tag{C1}$$

The quantities involved are defined after Eq. (39) in the main text. The Bloch functions u_{c0} and $u_{v0}^j (j = 1, 2, 3, 4)$ are normalized according to

$$\int_{V_\Omega} d^3\mathbf{r}|u(\mathbf{r})|^2 = V_\Omega, \tag{C2}$$

where V_Ω is the volume of the primitive cell. The link between the bond orbitals and the Bloch functions is given by the identity

$$u^j_{v0}(\mathbf{r}) = \sum_{\mathbf{R}} w_j(\mathbf{r}-\mathbf{R}) , \tag{C3}$$

valid for Wannier functions w_j.[42] To get the proper normalization of the Bloch functions we set

$$w_j(\mathbf{r}-\mathbf{R}) = \sqrt{V_\Omega}|\mathbf{R}, u^j_{m_j}> . \tag{C4}$$

Using Eqs. (C3) and (C4) we can transform the EBOM hole wave function $|\psi_h >= \sum_i D_i|\psi^\Gamma_i >= \sum_j G_j(\mathbf{R})|\mathbf{R}, u^j_{m_j}>$ to the effective-mass picture as follows:

$$\begin{aligned}|\psi_h> &= \sum_{\mathbf{R}j} G_j(\mathbf{R})|\mathbf{R}, u^j_{m_j}> \\ &= \sum_{\mathbf{R}j} \frac{G_j(\mathbf{R})}{\sqrt{V_\Omega}} w_j(\mathbf{r}-\mathbf{R}) \\ &\simeq \sum_j \psi^j_h(\mathbf{r}) \sum_{\mathbf{R}} w_j(\mathbf{r}-\mathbf{R}) \\ &= \sum_j \psi^j_h(\mathbf{r}) u^j_{v0}(\mathbf{r}).\end{aligned} \tag{C5}$$

Here $\psi^j_h(\mathbf{r})$ is a smooth function which interpolates $G_j(\mathbf{R})/\sqrt{V_\Omega}$ at all lattice points and corresponds to the effective-mass envelope function. The overlap integral in Eq. (C1) can now be evaluated as

$$\begin{aligned}\left|\int d^3\mathbf{r}\, \psi^j_h(\mathbf{r})\psi_e(\mathbf{r})\right|^2 &\simeq \left|\sum_{\mathbf{R}} V_\Omega \psi^j_h(\mathbf{R})\psi_e(\mathbf{R})\right|^2 \\ &= V_\Omega \left|\sum_{\mathbf{R}} G_j(\mathbf{R})\psi_e(\mathbf{R})\right|^2 .\end{aligned} \tag{C6}$$

The expression for f_x thus turns into

$$\begin{aligned}f_x = \frac{2}{mE_0} V_\Omega \sum_j |<u_{c0}|p_x|u^j_{v0}>|^2 \\ \times \left|\sum_{\mathbf{R}} G_j(\mathbf{R})\psi_e(\mathbf{R})\right|^2 .\end{aligned} \tag{C7}$$

For symmetry reasons only the basis functions labeled a and b in Eqs. (16) and (17) will contribute to the sum in Eq. (C7). This is because only these angular basis functions belong to the same irreducible representations (for the point group of the quantum well) as the electron basis functions. The expression for the oscillator strength for a j-like (Γ_6 or Γ_7) bound exciton to use in our combined EBOM and effective-mass approach thus simplifies to

$$\begin{aligned}f^j_x = \frac{2}{mE_0}|<u_{c0}|p_x|u^j_{v0}>|^2 V_\Omega \\ \times \left|\sum_{\mathbf{R}} G_j(\mathbf{R})\psi_e(\mathbf{R})\right|^2 ,\end{aligned} \tag{C8}$$

which is Eq. (41) in the main text.

APPENDIX D

The band offsets given in Eq. (43) imply that the ZnSe-$Zn_{1-x}Mn_xSe$ quantum well under consideration is weakly type II for the heavy holes and weakly type I for the light holes. Therefore, the single-particle states for the holes may not provide a good basis for solving the Schrödinger equation for the heavy-hole and light-hole excitons. In this appendix we extend the formalism by Sanders and Chang,[34] as modified by Wu and Nurmikko,[35] to treat weakly type-I and type-II excitons.

The Hamiltonian for the exciton is $H = H_e + H_h + v$, where H_e and H_h are the effective-mass Hamiltonians for the electron and hole, including the strain-induced changes in band offsets, and v is the Coulomb interaction. The single-particle hole states are calculated with a multiband effective-mass theory ($\mathbf{k}\cdot\mathbf{p}$), while the electron states are treated within the spherical effective-mass approximation. The material parameters are given in the main text. Because the heavy-hole single-particle states are spatially extended due to the type-II character of the band offset, they do not provide a useful basis for solving the excitonic Hamiltonian. Similarly, although the light hole is type I, the confinement is quite weak. However, in the presence of the electron-hole interaction, the single-particle hole states are better confined. We thus choose for the hole basis the set of hole eigenstates of appropriately chosen "artificial" quantum wells. This is done by modifying the heavy-hole and light-hole "effective" band edges by adding, in general, different potentials $\delta V_{\rm LH}$ and $\delta V_{\rm HH}$ to the hole part of the Hamiltonian when solving for the hole basis functions.

According to the standard method,[34] we obtain the following Schrödinger equation for the exciton in a two-band model, including one electron and one hole subband:

$$\begin{aligned}[E^e_n(\mathbf{k}_\parallel) - E^h_m(\delta V, \mathbf{k}_\parallel)]G_{nm}(\mathbf{k}_\parallel) \\ + \sum_{\mathbf{k}'_\parallel} V_{nm}(\delta V, \mathbf{k}_\parallel, \mathbf{k}'_\parallel)G_{nm}(\mathbf{k}'_\parallel) = E(\delta V)G_{nm}(\mathbf{k}_\parallel),\end{aligned} \tag{D1}$$

where δV symbolizes $\delta V_{\rm LH}$ and $\delta V_{\rm HH}$. Here $E^e_n(\mathbf{k}_\parallel)$ is the single-electron energy, $E^h_m(\delta V, \mathbf{k}_\parallel)$ is the expectation value of H_h in the hole basis which is in general different from the single-hole energy. $V_{nm}(\delta V, \mathbf{k}_\parallel, \mathbf{k}'_\parallel)$ is the corresponding Coulomb matrix element, and $G_{nm}(\mathbf{k}_\parallel)$ is the

excitonic envelope function. $G_{nm}(\mathbf{k}_{\|})$ is expanded in a set of 15 Gaussians with widths covering a broad physical range:

$$G_{nm}(\mathbf{k}_{\|}) = \sum_j C_{nm}^{\beta_j}(2\pi\beta_j)^{-1/2} \exp\left(-\frac{k_{\|}^2}{4\beta_j}\right). \quad \text{(D2)}$$

δV_{HH} and δV_{LH} are varied to give minimum ground-state energies for the light-hole and heavy-hole excitons. The exciton binding energies are found by subtracting the exciton energy from the sum of the single-particle electron and hole energies at the zone center ($\mathbf{k}_{\|} = \mathbf{0}$). (For the type-II heavy holes the single-particle energy corresponds to the barrier energy.)

The strain splits the heavy-hole and light-hole band edges by 44 meV. Thus, the results of our calculation for the light hole are close to those obtained by neglecting the band mixing. Because of the presence of strain, the heavy-hole states lie within the continuum of the light hole when the additional band offset δV_{HH} is included. As a result, the heavy-hole single-particle states interact with a continuum of light-hole states. This leads to fictitious resonances for the heavy-hole states. Nevertheless, because the heavy hole and the light hole are decoupled at the center of the Brillouin zone, it is sensible to think in terms of a heavy-hole subband, even though it lies in the light-hole continuum. A proper treatment of the band mixing with a continuum is beyond the scope of this study. Therefore the heavy-hole exciton is calculated neglecting the band mixing.

[1] W.T. Masselink and Y.-C. Chang, Phys. Rev. Lett. **51**, 509 (1983).

[2] B. Arfi, W.T. Masselink, and Y.-C. Chang, Phys. Rev. B **33**, 2401 (1986).

[3] A.Yu. Naumov, S.A. Permogorov, A.N. Reznitskii, V.Ya. Zhulai, V.A. Novozhilov, and G.T. Petrovskii, Fiz. Tverd. Tela (Leningrad) **29**, 377 (1987) [Sov. Phys. Solid State **29**, 215 (1987)].

[4] A.Reznitsky, S. Permogorov, S. Verbin, A. Naumov, Yu. Korostelin, V. Novozhilov, and S. Prokov'ev, Solid State Commun **52**, 13 (1984).

[5] I.V. Akimova, A.M. Akhekyan, V.I. Kozlovskii, Yu.V. Korostelin, and P.V. Shapkin, Fiz. Tverd. Tela (Leningrad) **27**, 1734 (1985) [Sov. Phys. Solid State **27**, 1041 (1985)].

[6] S. Permogorov, A. Reznitsky, S. Verbin, A. Naumov, W. von der Osten, and H. Stolz, J. Phys. (Paris) Colloq. **46**, C7-173 (1985).

[7] D. Lee, A. Mysyrowicz, A.V. Nurmikko, and B.J. Fitzpatrick, Phys. Rev. Lett. **58**, 1475 (1987).

[8] Q. Fu, D. Lee, A.V. Nurmikko, L.A. Kolodziejski, and R.L. Gunshor, Phys. Rev. B **39**, 3173 (1989). See also an earlier report from the same groups: L.A. Kolodziejski, R.L. Gunshor, Q. Fu, D. Lee, A.V. Nurmikko, J.M. Gonsalves, and N. Otsuka, Appl. Phys. Lett. **52**, 1080 (1988).

[9] Y.-C. Chang, Phys. Rev. B **37**, 8215 (1988).

[10] It is suggested in Ref. 8 that the repulsive potential felt by an electron corresponds to a conduction-band barrier of $\sim$ 0.5 eV. For the bound exciton the influence of this barrier can be estimated in perturbation theory, and the corrections turn out to be small (less than 0.5 meV).

[11] The electron-hole exchange interaction, left out in our model, is presumably small in the present system. For GaP:N, Arfi, Masselink, and Chang (Ref. 2) found the exchange energy to be less than 1 meV by using perturbation theory.

[12] G.T. Einevoll and Y.-C. Chang, Phys. Rev. B **41**, 1447 (1990).

[13] L.A. Kolodziejski, R.L. Gunshor, N. Otsuka, W.M. Becker, S. Datta, and A.V. Nurmikko, IEEE J. Quantum Electron. **QE-22**, 1666 (1986).

[14] An assumption of a less localized potential $V(\mathbf{r}_h)$ from the isoelectronic impurity, i.e., $< \mathbf{R}, \alpha|V(\mathbf{r}_h)|\mathbf{R}, \alpha >= V_1 \neq 0$ for $\mathbf{R}$ corresponding to sites that are nearest neighbors to the Te impurity, would presumably not change the results much since the parameter V_0 is fitted with the experimentally observed bound exciton binding energy. For GaP:N Arfi, Masselink, and Chang (Ref. 2) found the only effect to be a slight shift of the localized wave function from the impurity site to the nearest-neighbor sites.

[15] *Numerical Data and Functional Relationships in Science and Technology*, edited by K.H. Hellwege, Landolt-Börnstein Vol. 22a (Springer, New York, 1982).

[16] G.F. Koster, J.O. Dimmock, R.G. Wheeler, and H. Statz, *Properties of the Thirty-Two Point Groups* (MIT Press, Cambridge, MA, 1963).

[17] G.T. Einevoll and Y.-C. Chang, Phys. Rev. B **40**, 9683 (1989).

[18] L.A. Kolodziejski, R.L. Gunshor, T.C. Bonsett, R. Venkatasubramanian, S. Datta, R.B. Bylsma, W.M. Becker, and N.Otsuka, Appl. Phys. Lett. **47**, 169 (1985).

[19] Y. Hefetz, J. Nakahara, A.V. Nurmikko, L.A. Kolodziejski, R.L. Gunshor, and S. Datta, Appl. Phys. Lett. **47**, 989 (1985).

[20] M.-P. Houng and Y.-C. Chang, J. Appl. Phys. **65**, 3092 (1989).

[21] D.R. Yoder-Short, U. Debska, and J.K. Furdyna, J. Appl. Phys. **58**, 4056 (1985).

[22] A. Blacha, H. Presting, and M. Cardona, Phys. Status Solidi B **126**, 11 (1984).

[23] This can be seen directly, but follows also from a general group-theoretical matrix-element theorem [see, for example, p. 80 in M. Tinkham, *Group Theory and Quantum Mechanics* (McGraw-Hill, New York, 1966)].

[24] L. Oliveira, Phys. Rev. B **38**, 10 641 (1988).

[25] This follows from the generalized Unsöld theorem. See p. 80 in Ref. 23.

[26] F. Seitz, *The Modern Theory of Solids* (McGraw-Hill, New York, 1940).

[27] See, for example, C.H. Henry and K. Nassau, Phys. Rev. B **1**, 1628 (1970) and L.C. Andreani and A. Pasquarello, Europhys. Lett. **6**, 259 (1988). A nice derivation of the form of the optical matrix elements for excitons in quasi-two-dimensional systems can be found in G. Bastard, *Wave Mechanics Applied to Semiconductor Heterostructures* (Les Editions de Physique, Les Ulis, France, 1988).

[28] These values are the maximum values found when trying

out both directions of the electron spin. See G. Bastard, *Wave Mechanics Applied to Semiconductor Heterostructures* (Ref. 27), p. 248.
[29] U. Rössler and H.-R. Trebin, Phys. Rev. B **23**, 1961 (1981).
[30] P. Lawaetz, Phys. Rev. B **4**, 3460 (1971).
[31] A. Baldereschi and N.O. Lipari, Phys. Rev. B **3**, 439 (1971).
[32] Standard expressions for binding energy and expected radial distance for a hydrogenic donor: $E_b = (13.6\ \text{eV}) m_e/(m_0 \epsilon_0^2)$ and $a^* = (0.529\ \text{Å}) \epsilon_0 m_0/m_e$.
[33] A.V. Nurmikko (private communication).
[34] G.D. Sanders and Y.-C. Chang, Phys. Rev. B **35**, 1300 (1987).
[35] J.-W. Wu and A.V. Nurmikko, Phys. Rev. B **38**, 1504 (1988).
[36] See G. Bastard, in *Wave Mechanics Applied to Semiconductor Heterostructures* (Ref. 27), pp. 251–255.
[37] See any introductory text in quantum mechanics, for example, S. Gasiorowicz, *Quantum Physics* (Wiley, New York, 1974).
[38] J.J. Song, Y.S. Yoon, P.S. Jung, A. Fedotowsky, J.N. Schulman, C.W. Tu, J.M. Brown, D. Huang, and H. Morkoç, Appl. Phys. Lett. **50**, 1269 (1987).
[39] In Ref. 17 the EBOM was used to study a double acceptor in GaAs. After fitting the on-site value of the Coulombic impurity potential to get the correct ground-state energy (−203 meV), the EBOM predicted an excited state at −44 meV in good agreement with experiment. In the same study the EBOM also predicted the energy of the first even-parity excited state for the indium (In) impurity which has a binding energy of 157 meV. The predicted value for the binding energy of the excited state is 18.2 meV in good agreement with the experimental value at 19.2 meV. For the ground state of this acceptor the probability of finding the hole at the impurity site is $\sim 20\%$ which is comparable to what is encountered in the present calculation.
[40] See, for example, J.D. Jackson, *Classical Electrodynamics* (Wiley, New York, 1975), p. 102.
[41] See, for example, M. Rotenberg, R. Bivins, N. Metropolis, and J.K. Wooten, *The 3-j and 6-j Symbols* (Technology Press, Cambridge, MA, 1959).
[42] See, for example, W. Jones and N.M. March, *Theoretical Solid State Physics* (Wiley, London, 1973), Vol. 1.